






Fusing Ultra-Hyperspectral and High Spatial Resolution Information for Land Cover Classification Based on AISAIBIS Sensor and Phase Camera

Fangfang Qu , Shuo Shi , *Member, IEEE*, Zhongqiu Sun, Wei Gong , *Member, IEEE*, Biwu Chen , Lu Xu , Bowen Chen, and Xingtang Tang

Abstract—Hyperspectral imaging technology are widely used in vegetation, agriculture, and other fields, especially in land cover classification of complex scenes. Higher spectral resolution has become the focus of the development of hyperspectral imaging technology for classification. The advent of airborne AISAIBIS sensor reaches 0.11 nm ultrahyperspectral resolution. The ultrahyperspectral imagery shows great advantages in classification with its increasing spectral resolution. But its spatial resolution is limited because of the imaging mechanism, which brings great difficulties to the accurate extract of fine and regular objects. Therefore, we proposed an optimal fusion and classification strategy based on the complementary advantage information of ultrahyperspectral and high spatial resolution image. The fusion feasibility and effectiveness were verified by various fusion methods. And a quality evaluation system was developed to assess the quality of fusion results. Besides, a multiresolution segmentation optimization and classification evaluation scheme was proposed to comparatively analyze the effect of optimal fusion result on improving classification accuracy. Results show that the classification accuracy of the optimal fused image reaches 88.10%, and 7.11%–19.03% higher

than that of original images. It fully validates the effectiveness of the strategy proposed in this article.

Index Terms—AisaIBIS sensor, classification, fusion, phase camera, ultrahyperspectral resolution.

I. INTRODUCTION

HYPERSPECTRAL imaging technology plays a vital role in precision monitoring of agriculture, forestry management, environmental governance, detection of vegetation diseases, and other fields [1], [2], [3], [4], [5], [6], [7]. In particular, land cover classification is the basis and crucial part of the above-mentioned fields. Its development is more inseparable from hyperspectral remote sensing technology. In recent years, hyperspectral image classification received extensive attention in classification studies [8], [9]. It has become a significant way to promote the development of classification research with the data advantage of fast, large-scale, and high information dimension. For further precise land cover classification, hyperspectral sensor with higher instrument performance is urgently required. It poses extremely high challenges not only for spatial and spectral resolution, but also for the stability and accuracy of the system [10].

The advent of airborne AISAIBIS sensor has achieved ultrahyperspectral resolution of 0.11 nm. AISAIBIS sensor is the commercial application of the FLUO module of hyperspectral plant imaging spectrometer system for European Space Agency Earth Exploration Project (FIEX) [11]. The ultrahyperspectral image obtained by AISAIBIS sensor can provide richer and finer spectral information than existing public hyperspectral datasets [12], [13], [14], [15], [16], [17]. Rich spectral information brought by hyperspectral image provides many important features to ground object recognition. Therefore, it will play a huge role in improving the recognition accuracy of different objects in complex land cover scenarios.

However, the spatial resolution of the ultrahyperspectral image is greatly limited. Because the precise spectral resolution reduces the effective detection energy of each spectral band of the sensor, resulting in the performance decrease of parameters such as spatial resolution and signal-to-noise ratio. While finer spatial information is essential for maintaining the regularity and

Manuscript received 14 November 2022; revised 10 January 2023; accepted 17 January 2023. Date of publication 20 January 2023; date of current version 6 February 2023. This work was supported in part by the National Natural Science Foundation of China under Grant 41971307, in part by the Fundamental Research Funds for the Central Universities under Grant 2042022kf1200, in part by the Wuhan University Specific Fund for Major School-level Internationalization Initiatives, and in part by LIESMARS Special Research Funding. (Corresponding author: Shuo Shi.)

Fangfang Qu, Lu Xu, and Xingtang Tang are with the State Key Laboratory of Information Engineering in Surveying, Mapping and Remote Sensing, Wuhan University, Wuhan 430079, China (e-mail: fangqu@whu.edu.cn; xuluwh@whu.edu.cn; whutxt@whu.edu.cn).

Shuo Shi and Wei Gong are with the State Key Laboratory of Information Engineering in Surveying, Mapping and Remote Sensing, Wuhan University, Wuhan 430079, China, also with the Electronic Information School, Wuhan University, Wuhan 430072, China, and also with the Collaborative Innovation Center of Geospatial Technology, Wuhan 430079, China (e-mail: shishuo@whu.edu.cn; weigong@whu.edu.cn).

Zhongqiu Sun is with the Academy of Inventory and Planning, National Forestry and Grassland Administration, Beijing 100714, China (e-mail: sunzhongqiu@afip.com.cn).

Biwu Chen is with the Shanghai Radio Equipment Research Institute, Shanghai 201109, China (e-mail: cbw_think@whu.edu.cn).

Bowen Chen is with the State Key Laboratory of Information Engineering in Surveying, Mapping and Remote Sensing, Wuhan University, Wuhan 430079, China, and also with the Chinese Antarctic Center of Surveying and Mapping, Wuhan University, Wuhan 430079, China (e-mail: chenbowen1204@whu.edu.cn).

Digital Object Identifier 10.1109/JSTARS.2023.3238467

integrity of the object boundary, and the accurate identification of well-textured objects [18]. At present, there have been many studies of hyperspectral and high spatial resolution data fusion to solve the problem of the spatial resolution deficiencies in hyperspectral classification [19]. Fused images are considered to contain both advantages of high spatial and hyperspectral resolution images. Thereby it can provide richer spatial detail and spectral information for classification.

Chen et al. [20] carried out multisource remotely data fusion (hyperspectral, multispectral, and DEM) for land cover classification research. Results show that coarse-resolution data (hyperspectral) was superior to map detailed forest types after adding fine-resolution data (multispectral). Besides, Song et al. [21] used various fusion methods to conduct object recognition experiment based on multispectral and panchromatic data. Compared with multispectral image, the recognition accuracy of some ground objects was significantly improved after fusion. Yokoya et al. [22] compared and analyzed the effect of ten fusion methods based on hyperspectral and multispectral data fusion. Their performance of classification in different datasets was tested. It was found that Hysure method achieved the highest classification accuracy in Pavia University dataset. Further, some scholars have developed fusion strategies using deep learning methods [23].

In summary, various fusion researches show that: the land cover classification by fusing images with different spatial resolution is superior to that only using hyperspectral data. It can effectively supplement the problem of insufficient spatial information of hyperspectral data in ground object recognition [24]. However, whether these strategies are suitable for the fusion of ultrahyperspectral data and higher spatial resolution data remains to be verified.

In fusion research based on ultrahyperspectral and high spatial resolution data, the following points should be noticed.

- 1) The existing fusion strategies are susceptible to varying degrees of information loss [25]. Images with different resolutions not only contain redundant information to be removed, but also have complementary advantage information for classification. Information loss leads to the important features of original images not being maximum preserved [25], [26], [27].
- 2) The existing fusion methods lack an effective and uniform evaluation system. To assess the quality and robustness of the fused images, an appropriate evaluation mechanism is needed [28].
- 3) The object segmentation is an essential part in object-oriented classification [29]. The optimal settings of segmentation parameters vary greatly from data to data during the segmentation process [30].

This article proposed an optimal spatial-spectral information fusion strategy for classification based on high spatial resolution image from Phase camera and ultrahyperspectral resolution image from AISAIBIS sensor. The main contributions of this article were as follows: developing a variety of spatial-spectral information fusion strategies to solve the resolution inconsistency and mismatch of data sources from different sensors; building a quality evaluation system from the aspects of brightness, shape,

TABLE I
PARAMETER SETTINGS OF AISAIBIS SENSOR

Parameter Setting	Value Setting
Binning	2×2
Spectral sampling	0.11 nm
Frames per second (FPS)	60
Ground pixel size	1 m
Flight Altitude	1450 m
Spatial pixels	768
FPS Width	768 m

texture, and spectrum to evaluate the ability of fused images in retaining spatial detail and spectral advantage information of the original data; developing a multiresolution segmentation optimization scheme based on the spatial and spectral characteristics of different data sources to generate their optimal segments for classification; and using object-oriented classification method to compare the contribution of the data before and after fusion to the improvement of land cover classification. This article is believed to be valuable for further research of ultrahyperspectral image in fusion and land cover classification.

II. SYSTEM DESCRIPTION AND STUDY AREA

A. Airborne Campaign Based on AISAIBIS Sensor and Phase Camera

Airborne campaign was conducted between 03:00 and 04:00 (UTC TIME) on May 25, 2020, using AISAIBIS sensor (ultrahyperspectral imaging spectrometer) combined with Phase One iXU-RS 1000 aerial camera (high spatial resolution imaging equipment).

AISAIBIS sensors utilize SPECIM imaging spectrometer with high transmittance (F/1.7) and the new camera detection technology, sCMOS. It can maintain ultrahigh spectral sampling accuracy (0.11 nm) and excellent image quality. Its massive spectral information is particularly valuable for improving the accuracy of ground object recognition that has small differences. Besides, even in fast imaging flight conditions, AISAIBIS still has low noise, and high dynamic acquisition range. Table I gives the parameter settings of the AISAIBIS sensor during the flight campaign.

Phase camera provides high spatial resolution image with superior image quality. Its spatial resolution is as high as 0.133 m, which provides rich spatial detail information and texture information for different ground object identification in land cover classification. It is developed by industry-leading experts and technical teams. In terms of hardware, it can ensure compliance with the requirements of aerial photography of various scenes.

TABLE II
 PARAMETER SETTINGS OF PHASE CAMERA

Parameter Setting	Value Setting
Focal length (mm)	50.0
CCD pixel size (μm)	4.6
CCD Width ($\text{mm} \times \text{mm}$)	40.0568 \times 53.3968
Ground pixel size	0.133
Relative flying height	1450m

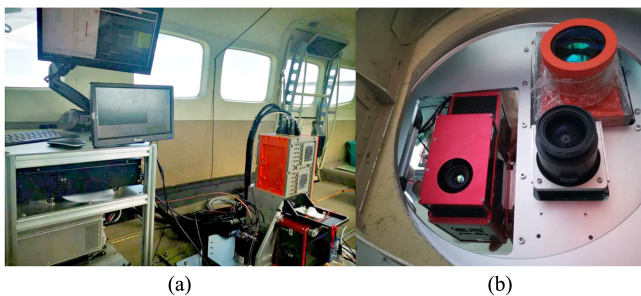


Fig. 1. Integration of airborne detection system. (a) System environment. (b) Installation and distribution of sensors.

In terms of software, it provides a variety of software solutions to seamlessly connect the entire acquisition and pre-processing process [31]. Table II gives the parameter settings of the phase camera during the flight campaign.

To ensure data acquisition process of the two sensors is synchronous, both sensors must be in the same coverage scene, climatic conditions, acquisition time, and lighting conditions. Therefore, we integrated the two sensors and fixed them to different locations of the same manned airborne detection device (see Fig. 1). On this basis, an inertial navigation system was added to record the flight trajectory.

B. Overview of the Study Area

The study area of this article is situated in Xiqing, central Danzhou City, Hainan Province, China [see Fig. 2(a)]. Geographically, it lies in latitudes between $19^{\circ}32'22''\text{N}$ and $19^{\circ}33'48''\text{N}$, and longitudes between $109^{\circ}25'50''\text{E}$ and $109^{\circ}26'31''\text{E}$. It covers a total area of 1.9 km^2 with an average altitude of 100m above the mean sea level.

The ground validation data [see Fig. 2(b)] was obtained through field surveys based on field sampling of the land-cover types. Based on the field surveys, the study site was classified into arbor forest (arbor), bamboo forest (bamboo), water body (water), construction land (construction), and wasteland.

In the entire experimental area, arbor land accounts for the highest proportion, covering more than 80%. Construction land

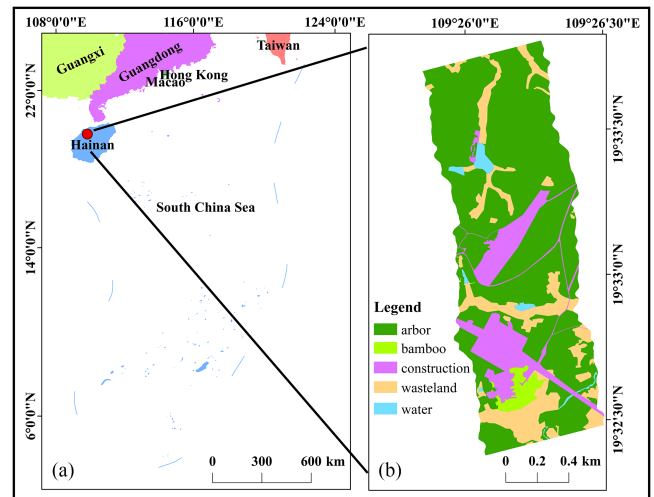


Fig. 2. Location of the study area. (a) Study area in Hainan Province. (b) Ground validation data of the study area.

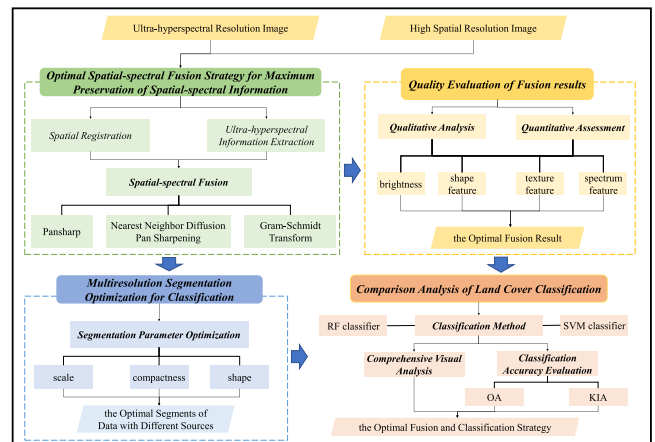


Fig. 3. Framework of fusing ultrahyperspectral and high spatial resolution information for classification based on phase camera and AISAIBIS sensor.

and bare land are secondary. In which the construction land mainly includes residential land, traffic land, and other lands for public facilities. Bare land is covered with a small amount of grass. Bamboo land and water body account for the lowest proportions, of which bamboo covers only one place, and water body covers six small places.

To be used in land cover classification, Training samples (1050 points) and test samples (450 points) were obtained by random sampling from ground validation data.

III. METHODS

The strategy of spatial-spectral fusion and classification based on high spatial resolution image from Phase camera and ultrahyperspectral resolution image from AISAIBIS sensor is presented in Fig. 3.

First, the spatial-spectral fusion experiments were carried out in three steps: spatial registration between images, and feature extraction; selection of fusion methods, and quality evaluation of fusion results. It used three fusion methods in this process,

including Pansharpen (PS), Gram–Schmidt (GS) transform, and nearest neighbor diffusion pan sharpening (NND) [32], [33], [34]. The best fusion result was filtered through subjective and quantitative analysis indicators. Then, the multiresolution segmentation optimization for classification evaluation was carried out in two steps.

- 1) Multiresolution segmentation optimization through constant adjustment of parameters combination [35].
- 2) Classification of the segments by support vector machine (SVM) classifier and random forest (RF) classifier, respectively.

Based on the classification results, comparative accuracy evaluation was conducted to further verify the effectiveness of the result of the optimal spatial-spectral information fusion strategy.

A. Strategy of Optimal Spatial-Spectral Information Fusion for Maximum Preservation of Spatial-Spectral Information

Different sensors have different physical properties and imaging principles. So that there is not a one-to-one correspondence between the ground objects in the resulting images of different sensors. This will not only exacerbate the spatial-spectral fusion error, but also seriously reduce the classification accuracy. Therefore, spatial geometry registration is necessary in this section. It is to match two or more images taken for the same object from different sensors, times, or angles. In this article, high spatial resolution image from Phase camera was taken as reference image. And ultrahyperspectral resolution image from AISAIBIS sensor was taken as image to be registered. To ensure a one-to-one correspondence between the ground objects of the reference image and image to be registered, 51 tie points were identified according to the invariance, uniqueness, stability, and independence. Based on those tie points, the quadratic polynomial correction model was selected to match images obtained by AISAIBIS sensor and phase camera [36].

However, spatial geometry registration only solves the image matching problem. The data redundancy generated by massive ultrahyperspectral and high spatial resolution information also has a significant impact on fusion quality and classification accuracy. Some studies have shown that abundant spectral information may bring about the “curse of dimensionality” [37]. Therefore, feature extraction is also an important part in this section. To achieve effective selection of key information from high-dimensional spectral features, we selected principal component analysis (PCA) as spectral feature extraction method. The spectral information of the image can be greatly preserved through this method.

The characteristics of different data sources differ widely. Their fusion requirements also vary widely. Therefore, methods selection for spatial-spectral fusion in this article is the main difficulty. This article selected three different fusion methods (PS, GS, and NND) to achieve the efficient fusion of advantage information of high spatial resolution image and ultrahyperspectral resolution image that is beneficial to classification.

PS is to calculate the relationship of the grey value of high spatial and ultrahyperspectral resolution images. It matches the grey value of the fusion band to the best by the least variance

technology [38]. Then, grey distribution of a single band is adjusted to reduce the color deviation of fused images [39]. It can realize the simultaneous fusion of multiple bands. Spectral and spatial features of the original images can also be well retained (that is high fidelity).

GS begins with the simulation of low spatial resolution Pan image based on high spatial and ultrahyperspectral resolution images [seen in (1)] [40]. Then, multidimensional linear orthogonal transformation is carried out based on simulated image and ultrahyperspectral image. After that, GS inverse transform is performed to get fused images [seen in (2)–(5)] [41]. For fused images obtained by this method, the components after the transformation are orthogonal. The order of the components is not sorted by the size of information contents. This method has high-fidelity characteristics. It also has no limits on the number of the original image bands. While this method usually takes longer time than other methods when the source data are large

$$P = \sum_{i=1}^k W_i \times B_i \quad (1)$$

where P is the gray value of the simulated image; i is the band number; k is the total number of bands; W is the weight; and B_i is the i th gray value of the hyperspectral image

$$GS_T(i, j) = (B_T(i, j) - \mu_T) - \sum_{i=1}^{T-1} \varphi(B_T, GS_i) \times GS_i(i, j) \quad (2)$$

where GS_T is the T th component after GS transformation; B_T is the T th band of the original ultrahyperspectral image; and μ_T is the mean gray value of the T th band of ultrahyperspectral image

$$\mu_T = \sum_{j=1}^C \sum_{i=1}^R B_T(i, j) / C \times R \quad (3)$$

$$\varphi(B_T, GS_i) = \sigma(B_T, GS_i) / \sigma(GS_i, GS_i)^2 \quad (4)$$

$$\sigma_T = \sqrt{\sum_{j=1}^C \sum_{i=1}^R (B_T(i, j) - \mu_T) / C \times R} \quad (5)$$

where $\varphi(B_T, GS_i)$ is the covariance of the T th band of ultrahyperspectral image; σ_T the sample standard deviation of the T -band of ultrahyperspectral image; C is the number of columns of the image; and R is the number of rows of the image.

NND is a method with high operation efficiency and high speed [42]. First, ultrahyperspectral resolution image is adjusted to the same spatial resolution as high spatial resolution image. Then spectral contribution vectors of the same frequency band number are obtained by linear regression. Finally, each pixel spectrum of fused image is weighted by adjacent pixels of the original hyperspectral image. The weight is determined by high spatial resolution image diffusion model [43]. Through this method, color distortion can be reduced. And the integrity of the spectrum before and after fusion can be preserved.

B. Quality Evaluation for Selection of the Optimal Spatial-Spectral Information Fusion Strategy

To assess the quality and robustness of fused images, this research separately selected two evaluation indexes: subjective and quantitative analysis. Subjective analysis mainly depends on visual comparison from spectrum, shape, and texture. Quantitative analysis is mainly represented by indicators based on rigorous mathematical models. Three indicators were selected for quantitative analysis: mean value indicator (AVG); standard deviation (STD); and correlation coefficient (CORR) [44].

AVG is used to evaluate image intensity. It is the arithmetic mean of grey values of all pixels in the image [seen in (6)]. If AVG is too large or too small, the brightness of the image will be affected

$$AVG = \frac{1}{M \times N} \sum_{i=1}^M \sum_{j=1}^N f(i, j) \quad (6)$$

where $f(i, j)$ represents gray value of each pixel, M is number of image pixel rows, and N is number of image pixel columns.

STD is an indicator for description of spatial information. If STD value is too small, the image contrast is not obvious, which means that some spatial details cannot be displayed. STD is defined as

$$STD = \sqrt{\frac{1}{M \times N} \sum_{i=1}^M \sum_{j=1}^N (f(i, j) - AVG)^2} \quad (7)$$

CORR reflects the correlation degree between images before and after fusion. Larger CORR means that the fused image is closer to original image, resulting in better spectral fidelity

$$CORR = \frac{\sum_{i=1}^M \sum_{j=1}^N [(f_{fus}(i, j) - AVG_{fus}) \times (f_{ori}(i, j) - AVG_{ori})]}{\sqrt{\sum_{i=1}^M \sum_{j=1}^N [(f_{fus}(i, j) - AVG_{fus})^2] \times \sum_{i=1}^M \sum_{j=1}^N [(f_{ori}(i, j) - AVG_{ori})^2]}} \quad (8)$$

where $f_{fus}(i, j)$ is pixel value of fused image, $f_{ori}(i, j)$ is pixel value of original image, AVG_{fus} is the mean pixel value of fused image, and AVG_{ori} is mean value of original image.

C. Optimization of Multiresolution Segmentation for Land Cover Classification

Multiresolution segmentation starts with a single pixel. It merges adjacent pixels of the single pixel into polygon objects. After that, adjacent objects are merged based on heterogeneity least principle. Repeat this step until all pixels are fused into the object. Eventually all pixels are converted into evenly distributed adjacent objects. In this process, the parameter settings determine the final segmentation quality. The parameter value is determined by not only the image characteristics, but also the geographical environment of the area.

Segmentation parameters include scale factor, shape factor, color factor, compactness factor, and smoothness factor (see Fig. 4) [45]. Scale factor affects the size of segments. High scale value leads to large objects. Lower scale value produces smaller objects, even fragmented objects [46]. Shape factor optimizes

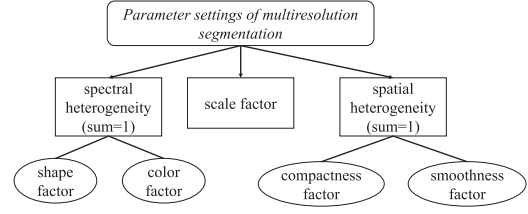


Fig. 4. Principle of parameter settings of multiresolution segmentation.

the spatial consistency of segments. It interacts with color factor. Color factor is closely related to spectral distribution. Over high weight of shape factor leads to the quality decrease of segments. Compactness factor interacts with smoothness factor to the optimization of object consistency. High weight of the compactness factor is benefit to objects with regular shape and complex structure.

D. Comparative Evaluation of Classification Based on the Optimal Spatial-Spectral Information Fusion Strategy

To verify whether the fused images are effective for improving the classification accuracy, we performed two popular machine-learning classifiers (SVM and RF) in this research, and analyzed the classification results. In addition, the confusion matrix was used to further evaluate the classification results of different classification methods, and to verify the effectiveness of the fusion optimization strategy.

SVM classifier is a supervised classification method [47]. Its principle is finding a hyperplane in a set of distributed decision boundaries at the beginning. In this hyperplane, classification error of the model is required very close to zero, especially classification error of the unknown dataset should be reduced as much as possible. Then objects are classified by finding the decision boundary with the largest boundary. This method has good robustness. Whether few samples or large redundant samples, it is always good at grasping key samples for training and classification. Besides, this method avoids “dimension disaster” to some degree [48].

RF classifier consists of many decision trees. The input data is required to be entered into each decision tree for classification. First, training samples are randomly selected using bootstrap sampling method. Then, feature subsets are randomly selected from all features. When each tree reaches its maximum, the classification process is over. There is no need to prune the decision tree during the process. This method is good at handling data with many features. It has strong resistance to overfitting [49].

In the classification process, both classifiers require a certain proportion of training samples and validation samples for classification. Therefore, we selected 1500 random points as samples based on the ground validation data. Ultimately, this article used 70% samples as training samples, and other 30% samples as validation samples.

Besides, to quantitatively assess the classification effectiveness of the optimal fusion result, accuracy evaluation is an effective way. Before calculating the classification accuracy,

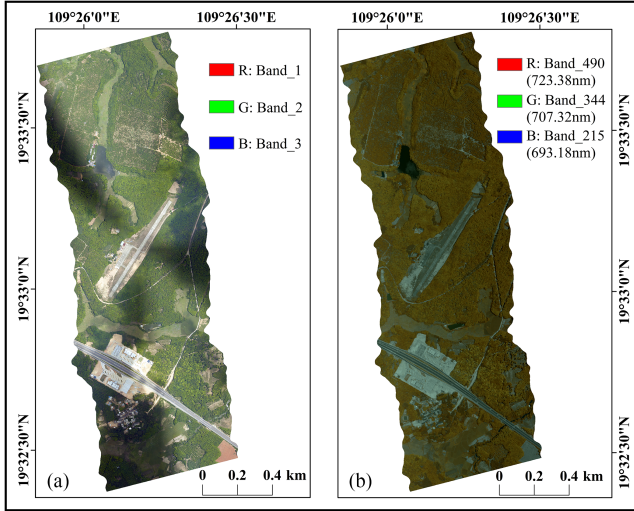


Fig. 5. Flight experiment results. (a) High spatial resolution image. (b) Ultrahyperspectral resolution image.

validation samples with sufficient proportion should be generated. The measurement of the classification effectiveness was generated by the overall accuracy (OA), and the Kappa index (KIA) based on the error matrix. OA is the ratio of the number of correctly classified samples to the number of all samples. KIA is calculated using the information of the entire error matrix. It is an indicator of the consistency test

$$OA = \frac{\sum_{i=1}^N x_{ii}}{n} \quad (9)$$

$$KIA = \frac{P_0 - P_c}{1 - P_c} \quad (10)$$

$$P_c = \frac{\sum_{j=1}^N \left(\sum_{i=1}^N x_{ji} * \sum_{i=1}^N x_{ij} \right)}{n^2} \quad (11)$$

where n is the total pixel numbers participating in the classification; N is the number of rows (or columns) of the error matrix; i is the row number of the error matrix; j is the column number of the error matrix; and P_0 is the value of OA.

IV. RESULTS

A. Acquisition Results of Ultrahyperspectral and High Spatial Resolution Images

Fig. 5(a) shows the high spatial resolution image obtained by Phase camera. It has 0.133 m spatial resolution and RGB bands. The ultrahyperspectral resolution image obtained by AISAIBIS sensor is shown in Fig. 5(b). It has 1004 bands with 0.11 m ultrahyperspectral resolution, and wavelength from 669.84 to 780.32 nm. Besides, both images complete the data preprocessing of atmospheric correction and radiation correction before the study.

The size of the high spatial resolution image is 9627×21968 . Its data volume is 806.75 MB. The ultrahyperspectral resolution image has a larger data volume (5.69 GB), with the size of 1155×2634 .

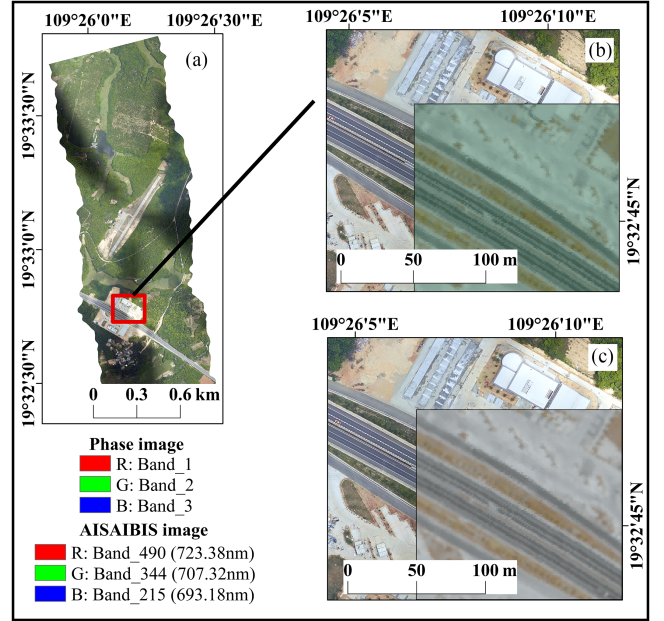


Fig. 6. (a) Location of the detailed display area in the high spatial resolution image. (b) Before image registration, (c) After image registration.

B. Selection of the Optimal Fusion Strategy for Maximum Spatial-Spectral Information Preservation

1) *Results of Spatial Registration and Ultrahyperspectral Information Extraction:* The results of the spatial geometry registration experiment are shown in Fig. 6. In the process of spatial geometry registration, the overall root mean square error of 51 tie points was controlled below 0.50 [50]. The comparison before image registration indicates that roads in two images do not overlap [see Fig. 6(b)]. After spatial registration, obvious geometric deviation of them was well eliminated [see Fig. 6(c)]. Roads in high spatial and ultrahyperspectral resolution images match exactly.

In spectral transformation step, 1004 bands of ultrahyperspectral resolution image are turned into 1004 principal components (PCs). All spectral information in the 1004 bands of ultrahyperspectral resolution image is sorted by spectral feature importance, which is included in each PC at different weights. To highlight meaningful parts of the spectral transformation result, we picked the eigenvalues of the first 10 PCs, which arranged in descending order of total eigenvalues [see Table III].

To get the final feature extraction results, we extracted the first 7 PCs of the transformation result of ultrahyperspectral resolution image. Based on the screen plot test, the feature extraction results include the inflection point (i.e., the indicators of that PC change are basically unchanging), and its previous points. From Table III, it can be clearly seen that the changes of indicators of PC7 and subsequent PCs tend to be stable.

2) *Quality Analysis of Fusion Results Based on Optimal Spatial-Spectral Information Fusion Strategy:* Fig. 7 shows fusion results of different methods based on high spatial and ultrahyperspectral resolution information. From visual comparison, it is shown that the results of all fusion methods

TABLE III
INDICATORS OF FEATURE EXTRACTION OF ULTRAHYPERSPECTRAL
RESOLUTION IMAGE

Principal Components	Eigenvalue		
	Total	Variance (%)	Cumulative Variance (%)
PC1	24111850889.53	89.9501	89.950
PC2	2637147835.51	9.8380	99.788
PC3	46118163.93	0.1720	99.960
PC 4	4258166.07	0.0159	99.976
PC 5	1857048.14	0.0069	99.983
PC 6	451580.45	0.0017	99.984
PC 7	360573.45	0.0013	99.986
PC 8	217871.25	0.0012	99.987
PC 9	76276.33	0.001	99.987
PC 10	55275.49	0.001	99.987

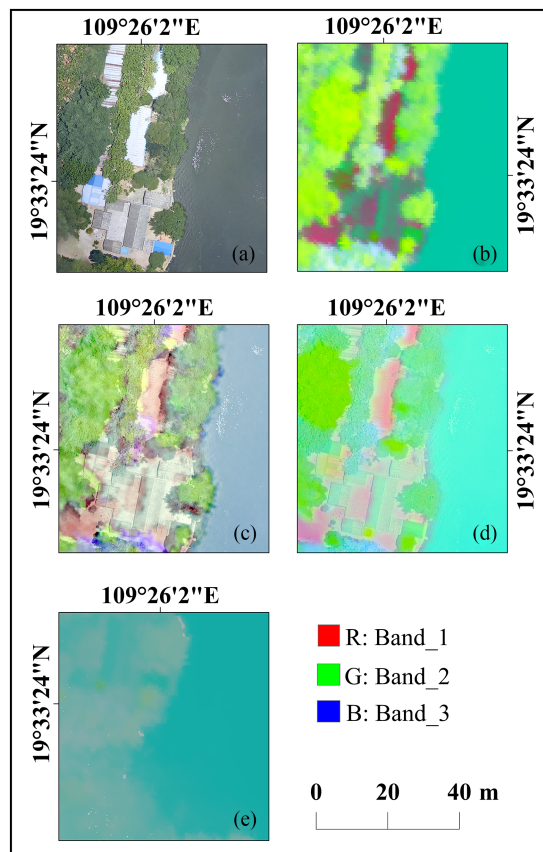


Fig. 8. (a) Original high spatial resolution image. (b) Feature extraction result of ultrahyperspectral resolution image, and the spatial-spectral fusion results. (c) PS result. (d) GS result. (e) NND result.

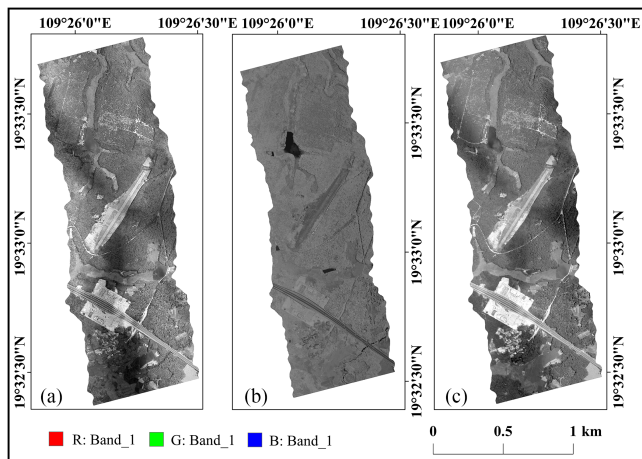


Fig. 7. Results of spatial-spectral fusion experiments with three different methods. (a) PS result. (b) NND result. (c) GS result.

(see Fig. 7) preserve the spatial shape information of the high spatial resolution image. But in spectral brightness aspect, fused images obtained by PS and GS methods have higher spectral fidelity than fused image of NND method. Besides, in spatial texture aspect, the result image obtained by GS method contains more texture information than others. The result image produced by NND method has a significant loss of texture information.

Further, we selected some detailed areas to clearly show the fusion outcomes of different fusion strategies through visual evaluation. They are shown in Fig. 8. As can be seen from

Fig. 8(a) and (b), the covering features of this scene are relatively complex, including water body, vegetation, construction land, and bare land. In high spatial resolution images, they have significant differences in spatial features. In the hyperspectral images after feature extraction, their spectral differences are also clear.

After fusion, it is found that all fusion methods have different levels of detail information loss. For the NND result, its information is lost seriously. It is almost impossible to recognize the above ground objects. In contrast, the PS and GS results completely retain the spatial and spectral information of the above kinds of ground objects. But the PS result is significantly affected by light and shadow, such as, the area around the trees. It leads to mixed spectral phenomena, which interferes with the recognition of ground objects and inhibits the accuracy of land cover classification. In summary, we think that the fusion result obtained by GS method are optimal to land cover classification.

For quantitative analysis, this article selects three indicators (see Table IV): AVG and STD based on the brightness value of images before and after fusion, and CORR based on the spectral information between ultrahyperspectral resolution image and fusion results. In brightness information aspect, AVG change trends of the result image of GS method is closer to that of ultrahyperspectral resolution image. In spatial information aspect, STD value of result image of NND method is the highest. It indicates that the result image of NND method contains more

TABLE IV
QUANTITATIVE EVALUATION OF THE FUSED IMAGES

Image Type	Band	AVG	STD	CORR
High spatial resolution image	1	97.458	48.990	/
	1	110252.526	74239.607	1
Ultra-hyperspectral resolution image	2	613.866	64708.269	1
	3	-296.111	8547.418	1
	4	-208.400	2578.169	1
	5	-57.519	1714.768	1
	6	-9.082	846.836	1
	7	-33.398	754.825	1
	PS	1	94003.881	93805.582
2		19730.474	22864.041	0.2614
3		3222.884	5810.795	0.4983
4		911.593	1513.503	0.3839
5		617.163	900.915	0.3290
6		330.195	579.606	0.3513
7		289.561	494.703	0.3196
GS	1	51340.012	89209.418	0.4033
	2	-7085.499	35207.215	0.6387
	3	-452.967	6582.975	0.7699
	4	-228.932	1952.724	0.7199
	5	-50.294	1323.500	0.9212
	6	-2.940	534.642	0.3105
	7	-35.113	533.552	0.5068
NND	1	177880.714	143501175.172	0.0020
	2	30891.463	40604772.880	0.0018
	3	3321.998	3854176.735	0.0061
	4	1434.089	1932945.412	0.0017
	5	1582.236	2162446.576	0.0044
	6	621.081	725339.341	0.0031
	7	301.435	408700.350	0.0001

spatial information than others. There may be an overfitting phenomenon in this method. In spectral information aspect, CORR value of GS and PS method are very close. While the correlation between the result image of NND method and the original image is weakest, which means that NND method causes serious spectral information loss. Therefore, we considered the GS method

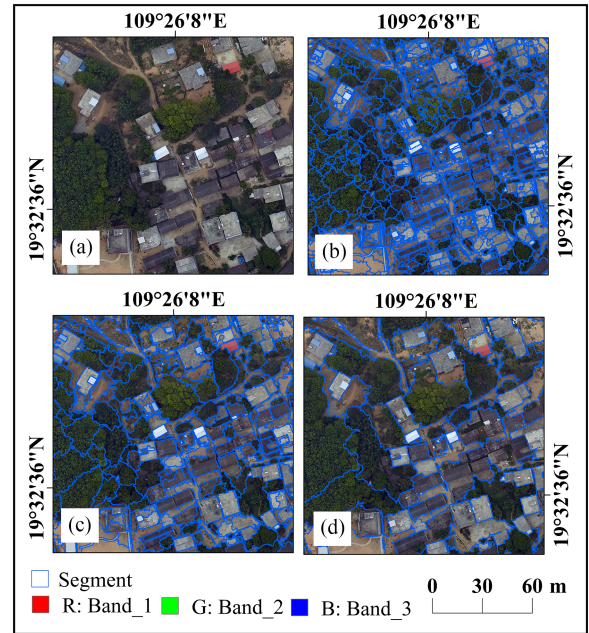


Fig. 9. (a) Original image and multiresolution segmentation results of the high spatial resolution image. (b) Parameter setting (scale: 50, shape: 0.3, and compactness: 0.5). (c) Parameter setting (scale: 100, shape: 0.3, and compactness: 0.5). (d) Parameter setting (scale: 300, shape: 0.3, and compactness: 0.5).

is superior to the PS method, and then superior to the NND method.

C. Analysis of Segmentation Optimization and Classification Results Based on the Optimal Fusion Result and Original Images

1) *Analysis of Segmentation Optimization Results:* In multiresolution segmentation experiment, scale factors were given 50, 100, 300, 500, 800, 1000, 3000, and 5000 [35]. Shape and compactness factors were given 0.1, 0.3, and 0.5, respectively. For example, the segmentation results under different scale factors (50, 100, and 300), the shape factor of 0.3 and the compactness factor of 0.5 are shown in Fig. 9.

The construction land of the selected area in Fig. 9 has highly complex spatial and spectral characteristics. There are arbor and bamboo forests mixed in. It is obvious that in Fig. 9(b), it occurs excessive segmentation. The segments are seriously broken and the objects after segmentation are very incomplete. In Fig. 9(d), the small arbor forests that hidden in the construction are not divided. All these conditions will increase the risk of misclassification of ground objects and inhibit the classification accuracy. In contrast, the segments in Fig. 9(c) obtained an excellent result. It is more suitable to the following land cover classification study. The optimal settings of the shape and compactness factors were also obtained at the same way.

Ultimately, the optimal parameter settings of every image were given in Table V, including the parameters of the fusion image, the original high spatial resolution image, and the original ultrahyperspectral resolution image. It is found that compactness setting of 0.5 is suitable to all images. While the optimal scale

TABLE V
OPTIMAL PARAMETER COMBINATIONS OF MULTIREOLUTION SEGMENTATION OF IMAGES BEFORE AND AFTER FUSION

Dataset	Parameter Sets		
	scale	shape	compactness
High spatial resolution image	100	0.3	0.5
Ultra-hyperspectral resolution image	300	0.3	0.5
Fusion image	3000	0.1	0.5

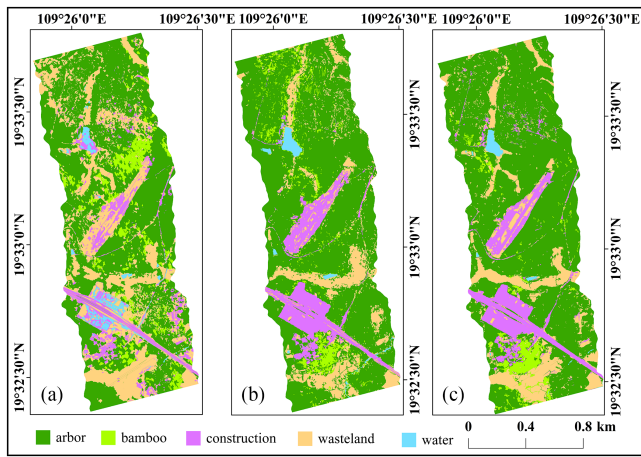


Fig. 10. Land cover classification results of SVM classifier. (a) High spatial resolution image. (b) Ultrahyperspectral resolution image. (c) Fusion image.

and shape factors for different images vary greatly. Because over high scale factor may lead to serious oversegmentation, resulting in the same object divided into multiple segments. Over low scale factor may lead to under-segmentation, which means two or more objects are grouped into the same segment [51].

As given in Table V, the optimum scale and shape combination for high spatial resolution image is 100:0.3. From multiresolution segmentation optimization result under this parameter setting in Fig. 9(c), it is observed that each class of different land-cover types of the image is grouped into individual objects without being too fragmented. For ultrahyperspectral resolution image, the optimal scale and shape combination is 300:0.3. And for the fusion image, segments can be satisfied only when the optimal scale and shape combination is 3000:0.1.

2) *Comparative Analysis of Classification Effectiveness Between the Optimal Fusion Result and Original Images:* Classification results of the fused image and the original images are presented in Figs. 9 and 10. For SVM classifier, its kernel type was “linear,” and the C parameter (the coefficient that minimizes the error function) was 2. For RF classifier, the tree number setting of it was 50, and its max features were 16.

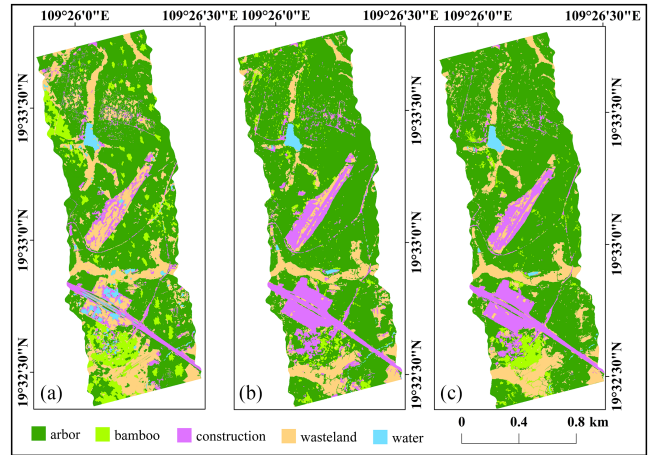


Fig. 11. Land cover classification results of RF classifier. (a) High spatial resolution image, (b) Ultrahyperspectral resolution image (c) Fusion image.

TABLE VI
CLASSIFICATION ACCURACIES FOR SVM AND RF CLASSIFIERS OF IMAGES BEFORE AND AFTER SPATIAL-SPECTRAL INFORMATION FUSION

Dataset	SVM classifier		RF classifier	
	OA (%)	KIA (%)	OA (%)	KIA (%)
High spatial resolution image	67.04	46.02	72.77	52.90
Ultra-hyperspectral resolution image	78.96	60.98	80.92	63.74
Fusion image	86.07	73.85	88.10	77.48

From Fig. 10(b) and (c) [or Fig. 11(b) and (c)], it is known that rich spectral features of the original ultrahyperspectral resolution image and the fusion image enhanced the identification of each class. In particular, the class of water body is well distinguished in the two images. By contrast, classification results of high spatial resolution image [see Figs. 10(a) and 11(a)] presented more and serious misclassification than others. For example, some arbor forest was classified into bamboo or wasteland. Many construction objects were misclassified as wasteland, and some other construction objects are mixed with water. The main reason for this phenomenon is lack of spectral information. In addition, there is a lot of impulse noise in classification results of the two original images. Arbor class of classification results of the two original images contains plenty of fragmented misclassified objects. This condition was well improved in fusion classification result.

Besides, we obtained the accuracy evaluation for classification results of images before and after fusion, which include OA and KIA indicators (see Table VI). The accuracy evaluation results indicate that SVM and RF classifiers get similar classification results. On the one hand, fusion image produced the best classification accuracy among all classified images.

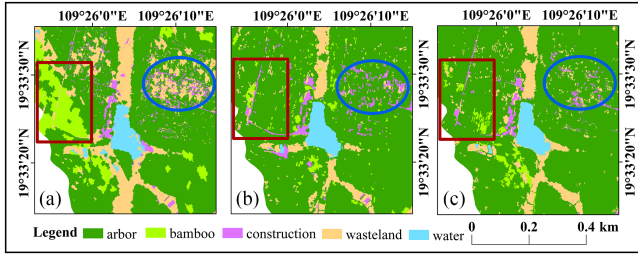


Fig. 12. Comparison of classification results from spectral perspective. (a) High spatial resolution image. (b) Ultrahyperspectral resolution image. (c) Fusion image.

It achieved 86.07% OA and 73.85% KIA with SVM classifier. And in RF classification, it achieved 88.10% OA and 77.48% KIA. The classification accuracy of fused image improved by 7.11%–19.03% compared with the original images. On the other hand, accuracy values of ultrahyperspectral resolution image are better than that of high spatial resolution image. Specifically, its OA was improved by 8.15%–11.92%.

Results in this article demonstrates that spatial-spectral information fusion can effectively improve the classification accuracy by combining advantage information of high spatial resolution image and ultrahyperspectral resolution image that is beneficial to classification.

V. DISCUSSION

To further analyze the effectiveness of the optimal fusion strategy in this article, we compared the image classification results before and after fusion from spectral perspective first. Fig. 12 shows the areas of arbor class with typical difference in different classification results. In the classification result of high spatial resolution image of Fig. 12(a), many large arbor objects were misclassified into bamboo and wasteland due to the lack of spectral information. Furthermore, there are some shadow areas at the time of the original image acquisition (see Fig. 5). Therefore, spatial features are overused to identify this part as bamboo forest during the classification process.

In contrast, the misclassification of arbor into other classes was significantly improved in the hyperspectral classification result of Fig. 12(b). It can be seen from the fusion image in Fig. 12(c) that, it fulfils the spectral advantage in classification, which not only improves the phenomenon of misclassification, but also greatly weakens the influence of the shadow of the original high spatial resolution image on the classification accuracy. Most of the shaded arbor areas were identified. It is obvious that the advantages of spectral features of that image are more superior to spatial features in this classification scene.

Through further analysis, we found that the addition of massive spatial information in the process of object recognition can more accurately distinguish the boundary of different objects. It is liable to accurately distinguish the classes with significantly different spatial feature. The spatial information used in this article consists of two parts, spatial geometry information and spatial texture information. Here we take the Y-shaped wasteland in Fig. 13 as an example to analyze. The original high spatial

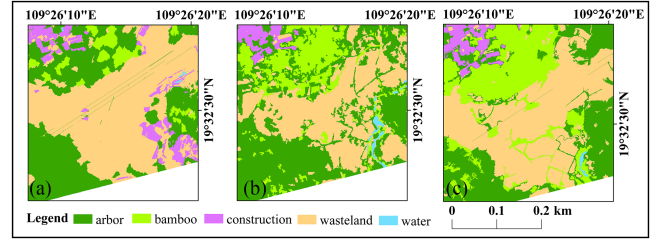


Fig. 13. Comparison of classification results from spatial perspective. (a) High spatial resolution image. (b) Ultrahyperspectral resolution image. (c) Fusion image.

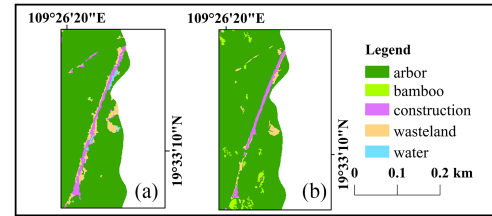


Fig. 14. Comparison of the road of construction land between classification results from spatial perspective. (a) Ultrahyperspectral resolution image. (b) Fusion image.

resolution image [see Fig. 13(a)] and the fused image [see Fig. 13(c)] have richer spatial information than the original ultrahyperspectral resolution image [see Fig. 13(b)]. It can be seen there are clear regular boundaries between their classification results of wasteland and arbor.

Besides, we selected a road in the study area, which is shown in Fig. 14. It is known that roads of construction land often have typical spatial features in remote sensing images. Before classification, it can be seen the road is surrounded by arbor forests from the original image (see Fig. 5). Furthermore, the image acquisition time is in the morning of local time. Trees on both sides of the road are unavoidably shaded by lighting, causing the acquired road data to be obscured by shadows. Ultrahyperspectral image uses its finer spectral information to identify this part of the shadow as wasteland. After analyzed, it believes that this part produced a shadow spectral signal that is close to the spectral information of road.

For fused image, it was classified using a combination of spatial and spectral information. Because of the introduction of finer spatial features, it extracted this section of the road in its entirety. It showed the effect of clear boundary. This confirms that the optimal fusion strategy proposed in this article preserved the spatial advantage information of the original data, especially the spatial detail information. It largely removed the interference of redundant parts from massive spatial and spectral information.

VI. CONCLUSION

This article explores and validates the optimal fusion strategy of high spatial and ultrahyperspectral resolution information, and the spatial-spectral fusion to the improvement of the classification accuracy. It is concluded that the spatial-spectral fusion strategy if our research can preserve the spatial and spectral

information of the original images very well. Applying the optimal fusion result to classification, it is considered that the classification accuracy of the fused image can be greatly improve. In summary, the ultrahyperspectral resolution image of our research is worth of further studying in the application of fusion, precise classification, and even tree species identification.

ACKNOWLEDGMENT

We gratefully acknowledge the Academy of Inventory and Planning, National Forestry and Grassland Administration for their help in data acquisition. We also acknowledge algorithms provided by eCognition software.

REFERENCES

- [1] X. Luo, X. Tong, Z. Qian, H. Pan, and S. Liu, "Detecting urban ecological land-cover structure using remotely sensed imagery: A multi-area study focusing on metropolitan inner cities," *Int. J. Appl. Earth Observ. Geo-Inf.*, vol. 75, pp. 106–117, 2019.
- [2] C. Nendel, Y. Hu, and T. Lakes, "Land-use change and land degradation on the Mongolian plateau from 1975 to 2015—A case study from Xilin-gol, China," *Land Degradation Develop.*, vol. 29, no. 6, pp. 1595–1606, 2018.
- [3] M. C. A. Picoli et al., "Big earth observation time series analysis for monitoring Brazilian agriculture," *ISPRS J. Photogramm. Remote Sens.*, vol. 145, pp. 328–339, 2018.
- [4] S. Shi et al., "Land cover classification with multispectral LiDAR based on multi-scale spatial and spectral feature selection," *Remote Sens.*, vol. 13, no. 20, 2021, Art. no. 4118.
- [5] S. Shi et al., "A convolution neural network for forest leaf chlorophyll and carotenoid estimation using hyperspectral reflectance," *Int. J. Appl. Earth Observ. Geo-Inf.*, vol. 108, 2022, Art. no. 102719.
- [6] M. Shimoni, R. Haelterman, and C. Perneel, "Hyperspectral imaging for military and security applications: Combining myriad processing and sensing techniques," *IEEE Geosci. Remote Sens. Mag.*, vol. 7, no. 2, pp. 101–117, Jun. 2019.
- [7] L. Xu et al., "Improving leaf chlorophyll content estimation through constrained PROSAIL model from airborne hyperspectral and LiDAR data," *Int. J. Appl. Earth Observ. Geo-Inf.*, vol. 115, 2022, Art. no. 103128.
- [8] S. Bhatti et al., "Site-specific irrigation management in a sub-humid climate using a spatial evapotranspiration model with satellite and airborne imagery," *Agricultural Water Manage.*, vol. 230, 2020, Art. no. 105950.
- [9] R. Hang, Q. Liu, D. Hong, and P. Ghamisi, "Cascaded recurrent neural networks for hyperspectral image classification," *IEEE Trans. Geosci. Remote Sens.*, vol. 57, no. 8, pp. 5384–5394, Aug. 2019.
- [10] J. Jia, Y. Wang, J. Chen, R. Guo, R. Shu, and J. Wang, "Status and application of advanced airborne hyperspectral imaging technology: A review," *Infrared Phys. Technol.*, vol. 104, 2020, Art. no. 103115.
- [11] B. Siegmund et al., "The high-performance airborne imaging spectrometer HyPlant—From raw images to top-of-canopy reflectance and fluorescence products: Introduction of an automatized processing chain," *Remote Sens.*, vol. 11, no. 23, 2019, Art. no. 2760.
- [12] M. Chen, Q. Wang, and X. Li, "Discriminant analysis with graph learning for hyperspectral image classification," *Remote Sens.*, vol. 10, no. 6, 2018, Art. no. 836.
- [13] N. Kakhani and M. Mokhtarzade, "A new neuro-fuzzy-based classification approach for hyperspectral remote sensing images," *J. Earth Syst. Sci.*, vol. 128, no. 2, pp. 1–21, 2019.
- [14] J. M. P. Nascimento and J. M. B. Dias, "Vertex component analysis: A fast algorithm to unmix hyperspectral data," *IEEE Trans. Geosci. Remote Sens.*, vol. 43, no. 4, pp. 898–910, Apr. 2005.
- [15] A. Plaza, P. Martínez, J. Plaza, and R. Pérez, "Dimensionality reduction and classification of hyperspectral image data using sequences of extended morphological transformations," *IEEE Trans. Geosci. Remote Sens.*, vol. 43, no. 3, pp. 466–479, Mar. 2005.
- [16] R. Zhang and J. Ma, "Feature selection for hyperspectral data based on recursive support vector machines," *Int. J. Remote Sens.*, vol. 30, no. 14, pp. 3669–3677, 2009.
- [17] W. Zhao, Z. Guo, J. Yue, X. Zhang, and L. Luo, "On combining multiscale deep learning features for the classification of hyperspectral remote sensing imagery," *Int. J. Remote Sens.*, vol. 36, no. 13, pp. 3368–3379, 2015.
- [18] R. Dian, S. Li, B. Sun, and A. Guo, "Recent advances and new guidelines on hyperspectral and multispectral image fusion," *Inf. Fusion*, vol. 69, pp. 40–51, 2021.
- [19] Z. Wang, B. Chen, R. Lu, H. Zhang, H. Liu, and P. K. Varshney, "Fusion-Net: An unsupervised convolutional variational network for hyperspectral and multispectral image fusion," *IEEE Trans. Image Process.*, vol. 29, pp. 7565–7577, 2020.
- [20] B. Chen, B. Huang, and B. Xu, "Multi-source remotely sensed data fusion for improving land cover classification," *ISPRS J. Photogramm. Remote Sens.*, vol. 124, pp. 27–39, 2017.
- [21] S. Song, J. Liu, H. Pu, Y. Liu, and J. Luo, "The comparison of fusion methods for HSRRSI considering the effectiveness of land cover (features) object recognition based on deep learning," *Remote Sens.*, vol. 11, no. 12, 2019, Art. no. 1435.
- [22] N. Yokoya, C. Grohnfeldt, and J. Chanussot, "Hyperspectral and multi-spectral data fusion: A comparative review of the recent literature," *IEEE Geosci. Remote Sens. Mag.*, vol. 5, no. 2, pp. 29–56, Jun. 2017.
- [23] Q. Feng, D. Zhu, J. Yang, and B. Li, "Multisource hyperspectral and LiDAR data fusion for urban land-use mapping based on a modified two-branch convolutional neural network," *ISPRS Int. J. Geo-Inf.*, vol. 8, no. 1, 2019, Art. no. 28.
- [24] L. Jian-Hua, "A comparative study of six methods for the fusion of QuickBird multispectral and pan images in consideration of segmentation effect," *Remote Sens. Land Resour.*, vol. 22, no. 3, pp. 21–25, 2010.
- [25] P. Zhao, S. Zhang, J. Liu, and H. Liu, "Zero-shot learning via the fusion of generation and embedding for image recognition," *Inf. Sci.*, vol. 578, pp. 831–847, 2021.
- [26] S. Eghbalian and H. Ghassemian, "Multi spectral image fusion by deep convolutional neural network and new spectral loss function," *Int. J. Remote Sens.*, vol. 39, no. 12, pp. 3983–4002, 2018.
- [27] J. Ma, W. Yu, C. Chen, P. Liang, X. Guo, and J. Jiang, "Pan-GAN: An unsupervised pan-sharpening method for remote sensing image fusion," *Inf. Fusion*, vol. 62, pp. 110–120, 2020.
- [28] S. C. Kulkarni and P. P. Rege, "Pixel level fusion techniques for SAR and optical images: A review," *Inf. Fusion*, vol. 59, pp. 13–29, 2020.
- [29] M. E. Sotille et al., "UAV-based classification of maritime Antarctic vegetation types using GEOBIA and random forest," *Ecol. Inform.*, vol. 71, 2022, Art. no. 101768.
- [30] M. D. Hossain and D. Chen, "Segmentation for object-based image analysis (OBIA): A review of algorithms and challenges from remote sensing perspective," *ISPRS J. Photogramm. Remote Sens.*, vol. 150, pp. 115–134, 2019.
- [31] G. Gabara and P. Sawicki, "Quality evaluation of 3D building models based on low-altitude imagery and airborne laser scanning point clouds," *Int. Arch. Photogramm., Remote Sens. Spatial Inf. Sci.*, vol. 43, pp. 345–352, 2021.
- [32] W. Sun, B. Chen, and D. Messinger, "Nearest-neighbor diffusion-based pan-sharpening algorithm for spectral images," *Opt. Eng.*, vol. 53, no. 1, 2014, Art. no. 013107.
- [33] V. Yilmaz, C. S. Yilmaz, O. Güngör, and J. Shan, "A genetic algorithm solution to the Gram-Schmidt image fusion," *Int. J. Remote Sens.*, vol. 41, no. 4, pp. 1458–1485, 2020.
- [34] Y. Zhang, "A new automatic approach for effectively fusing landsat 7 as well as IKONOS images," in *Proc. IEEE Int. Geosci. Remote Sens. Symp.*, vol. 4, 2002, pp. 2429–2431.
- [35] *eCognition Developer 9.0.1 Reference Book*. Munich, Germany: Trimble, 2014.
- [36] J. Wang, Y. Ge, G. B. Heuvelink, C. Zhou, and D. Brus, "Effect of the sampling design of ground control points on the geometric correction of remotely sensed imagery," *Int. J. Appl. Earth Observ. Geo-Inf.*, vol. 18, pp. 91–100, 2012.
- [37] J. Feng, L. C. Jiao, X. Zhang, and T. Sun, "Hyperspectral band selection based on trivariate mutual information and clonal selection," *IEEE Trans. Geosci. Remote Sens.*, vol. 52, no. 7, pp. 4092–4105, Jul. 2014.
- [38] X. Lirong and K. Jun, "Remote sensing image fusion based on PCA transform and wavelet transform," *Infrared Laser Eng.*, vol. 43, no. 7, pp. 2335–2340, 2014.
- [39] A. G. Snehmani, A. Ganju, S. Kumar, P. Srivastava, and H. R. R. P., "A comparative analysis of pansharpening techniques on QuickBird and WorldView-3 images," *Geocarto Int.*, vol. 32, no. 11, pp. 1268–1284, 2017.
- [40] B. Yu, "Geometric correction and fusion research on domestic satellite GF-1 data," 2015.
- [41] T. Maurer, "How to pan-sharpen images using the gram-schmidt pan-sharpen method—A recipe," 2013.
- [42] L. Kun, F. Jingying, and L. Fei, "Evaluation study of four fusion methods of GF-1 PAN and multi| spectral images," *Remote Sens. Technol. Appl.*, vol. 30, no. 5, pp. 980–986, 2015.

- [43] J. Zhao, L. Huang, H. Yang, D. Zhang, Z. Wu, and J. Guo, "Fusion and assessment of high-resolution WorldView-3 satellite imagery using NNDiffuse and Brovey algorithms," in *Proc. IEEE Int. Geosci. Remote Sens. Symp.*, 2016, pp. 2606–2609.
- [44] C. Liu, Y. Qi, and W. Ding, "Infrared and visible image fusion method based on saliency detection in sparse domain," *Infrared Phys. Technol.*, vol. 83, pp. 94–102, 2017.
- [45] J. Liu, M. Du, and Z. Mao, "Scale computation on high spatial resolution remotely sensed imagery multi-scale segmentation," *Int. J. Remote Sens.*, vol. 38, no. 18, pp. 5186–5214, 2017.
- [46] W. Yu, W. Zhou, Y. Qian, and J. Yan, "A new approach for land cover classification and change analysis: Integrating backdating and an object-based method," *Remote Sens. Environ.*, vol. 177, pp. 37–47, 2016.
- [47] S. Suthaharan, "Support vector machine-machine learning models and algorithms for big data classification," *Integr. Ser. Inf. Syst.*, vol. 36, pp. 207–235, 2016.
- [48] P. Liu, K.-K. R. Choo, L. Wang, and F. Huang, "SVM or deep learning? A comparative study on remote sensing image classification," *Soft Comput.*, vol. 21, no. 23, pp. 7053–7065, 2017.
- [49] A. Reyes, M. Solla, and H. Lorenzo, "Comparison of different object-based classifications in LandsatTM images for the analysis of heterogeneous landscapes," *Measurement*, vol. 97, pp. 29–37, 2017.
- [50] S. Periaswamy and H. Farid, "Medical image registration with partial data," *Med. Image Anal.*, vol. 10, no. 3, pp. 452–464, 2006.
- [51] M. Imani and H. Ghassemian, "An overview on spectral and spatial information fusion for hyperspectral image classification: Current trends and challenges," *Inf. Fusion*, vol. 59, pp. 59–83, 2020.



Fangfang Qu received the B.S. degree in geographic information science from the School of Earth Sciences, Yangtze University, Wuhan, China, in 2020. She is currently working toward the MA.Eng. degree in resources and environment with the State Key Laboratory of Information Engineering in Surveying, Mapping, and Remote Sensing, Wuhan University, Wuhan, China.

Her research interests include hyperspectral image and lidar data processing, multisource remote sensing data fusion, hyperspectral data classification and segmentation, and fluorescence data application.



Shuo Shi (Member, IEEE) received the Ph.D. degree in photogrammetry and remote sensing from Wuhan University, Wuhan, China, in 2015.

He is currently an Associate Professor with the State Key Laboratory of Information Engineering in Surveying, Mapping and Remote Sensing, Wuhan University. He has been supported the "Wuhan Morning Light Plan of Youth Science and Technology." He has authored or coauthored more than 30 peer reviewed research articles. His research interests include hyperspectral lidar, fluorescence lidar, true color imaging, target classification, and vegetation quantitative remote sensing.



Zhongqiu Sun received the Ph.D. degree in cartography and geography information system from Peking University, Beijing, China, in 2016.

She is currently a Senior Engineer with the Academy of Inventory and Planning, National Forestry and Grassland Administration, Beijing, China. Her research interests include ultrahyperspectral data processing, hyperspectral lidar, land use classification, and forest resources monitoring.



Wei Gong (Member, IEEE) received the B.S. degree in photonics engineering and the Ph.D. degree in physical electronics from the Huazhong University of Science and Technology, Wuhan, China, in 1993 and 1999, respectively, and the M.S. degree in electronics from the Chinese Academy of Science, Lanzhou, China, in 1996.

From 2002 to 2004, he was an Assistant Professor with Hampton University, Hampton, VA, USA. From 2004 to 2020, he was a Professor with the State Key Laboratory of Information Engineering in Surveying, Mapping and Remote Sensing, Wuhan University, Wuhan, China. He is currently the Dean of the School of Electronic Information, Wuhan University. In recent years, he has more than 100 scientific papers accepted and published, 18 patents, and two books coauthored. He is mainly engaged in teaching and research of new lasers, optical technology, and its remote sensing applications, and has made achievements in atmospheric lidar and optical remote sensing.

Dr. Gong was selected as one of the New Century Excellent Talents in 2007, LuoJia Scholars and Chutian Scholars in 2010, and Yangtze River Scholars in 2014.



Biwu Chen received the B.S. degree in remote sensing science and technology from the School of Remote Sensing and Information Engineering, Wuhan University, Wuhan, China, in 2015 and the Ph.D. degree in photogrammetry and remote sensing from the State Key Laboratory of Information Engineering in Surveying, Mapping, and Remote Sensing, Wuhan University.

His research interests include hyperspectral lidar data processing, point cloud classification and segmentation.



Lu Xu received the B.E. degree in resource exploration engineering from the School of Earth Resources, China University of Geosciences, Wuhan, China, in 2018. She is currently working toward the Ph.D. degree with the State Key Laboratory of Information Engineering in Surveying, Mapping and Remote Sensing, Wuhan University, Wuhan, China.

Her research interest includes deep learning, remote sensing, and land use classification.



Bowen Chen received the MA.Eng. degree in surveying and mapping engineering in 2020 from the State Key Laboratory of Information Engineering in Surveying, Mapping, and Remote Sensing, Wuhan University, Wuhan, China, where he is currently working toward the Ph.D. degree with the Chinese Antarctic Center of Surveying and Mapping, Wuhan, China.

His research interests include true-color 3-D imaging using hyperspectral light detection and ranging data.



Xingtao Tang received the B.E. degree in measurement and control technology and instrumentation from the School of Mechanical and Electronic Engineering, Wuhan University of Technology, Wuhan, China, in 2020. He is currently working toward the MA.Eng degree in resources and environment with the State Key Laboratory of Information Engineering in Surveying, Mapping, and Remote Sensing, Wuhan University, Wuhan, China.

His research interests include hyperspectral lidar data processing, point cloud classification, and vegetation carbon storage monitoring.